


Chern number and Hall conductivity in three-dimensional quantum Hall effect in Weyl semimetalsMingqi Chang ^{1,*}, Rong Ma,² and Li Sheng^{3,4,†}¹*Interdisciplinary Center for Fundamental and Frontier Sciences, Nanjing University of Science and Technology, Jiangyin, Jiangsu 214443, China*²*Jiangsu Key Laboratory for Optoelectronic Detection of Atmosphere and Ocean, Nanjing University of Information Science and Technology, Nanjing 210044, China*³*National Laboratory of Solid State Microstructures and Department of Physics, Nanjing University, Nanjing 210093, China*⁴*Collaborative Innovation Center of Advanced Microstructures, Nanjing University, Nanjing 210093, China*

(Received 10 April 2023; revised 14 July 2023; accepted 10 October 2023; published 20 October 2023)

The three-dimensional (3D) quantum Hall effect (QHE) in topological semimetals has attracted much interest in recent years. We study the 3D QHE in Weyl semimetals combining the Chern number calculated from Landau levels and the Hall conductivity calculated using the Kubo formula from the bulk-edge correspondence. We derive the Chern numbers under magnetic field using topological analysis. We get the magnetic field and Fermi energy dependence of the Hall conductivity according to the correspondence between the Chern number and Hall conductivity in a Weyl semimetal slab with the periodic boundary condition from the perspective of bulk states. We numerically calculate the Hall conductivity using the Kubo formula in a Weyl semimetal slab with the open boundary condition. The results of the Hall conductivity using the periodic boundary condition and open boundary condition are consistent. Our study demonstrates the 3D QHE in Weyl semimetals from both the bulk states and edge states through the bulk-edge correspondence.

DOI: [10.1103/PhysRevB.108.165416](https://doi.org/10.1103/PhysRevB.108.165416)**I. INTRODUCTION**

The discovery of the quantum Hall effect (QHE) in two-dimensional (2D) electron gas opens a frontier in condensed matter physics [1]. The subsequent study of topological states of matter has greatly enriched the development of condensed matter physics [2–5]. To generalize the 2D QHE to three dimensions, great efforts have been made for the last three decades [6–23]. In recent years, the three-dimensional (3D) QHE in topological semimetals has attracted intense interest [11–23].

Weyl semimetals are new topological states of matter in which the low-energy bulk states can be described by the Weyl equation [24–33]. The energy spectrum of the Weyl equation touches at discrete point, which are called Weyl nodes. The topologically protected surface states between the Weyl nodes form Fermi arcs, which is the landmark feature of Weyl semimetals [24]. It has been proposed that in a Weyl semimetal with two Weyl nodes, the Fermi arcs at two opposite surfaces can be connected by the Weyl nodes via a “wormhole” tunneling forming a complete Fermi loop producing the QHE [11]. Soon after the theoretical prediction, this unique 3D QHE was experimentally observed in the Dirac semimetal Cd_3As_2 [34–40]. To understand the 3D QHE in topological semimetals, it is explained from the perspective of Fermi arc surface states and bulk states, respectively [11–13,15,16,18]. Qin *et al.* explained the 3D QHE in Dirac

semimetals from the edge states in Ref. [15]. Li *et al.* elucidated a global picture of the edge states in Weyl semimetals in Ref. [16]. Moreover, Ma *et al.* numerically calculated the QHE in Weyl semimetals from the bulk states in Ref. [19]. In our previous work [20], we analytically calculated the Hall conductivity according to the Chern number from the perspective of bulk states. As is known, the nontrivial bulk topological invariant will result in the topological edge states emerging at the edges or boundaries of the system. This relationship between the bulk states and the edge states has been called the bulk-edge correspondence, originally introduced for the quantum Hall effect [41]. However, the theories of 3D QHE in Weyl semimetals combining the bulk states and edge states from the bulk-edge correspondence are still awaited.

In this paper, we study the 3D QHE in Weyl semimetals combining the bulk states and edge states through the bulk-edge correspondence. We analytically calculate the Chern numbers of a Weyl semimetal slab with the periodic boundary condition from Landau levels and numerically calculate the Hall conductivities with the open boundary condition using the Kubo formula. First, we calculate the Chern number of a Weyl semimetal without magnetic field. Then we calculate the Landau levels of the Weyl semimetal in a magnetic field. Through topological analysis, we get the distribution of the Chern number of Weyl semimetals in a magnetic field. In a Weyl semimetal slab with the periodic boundary condition, the Hall conductivity is calculated according to the correspondence between the Chern number and Hall conductivity. Meanwhile, the Hall conductivity is calculated numerically using the Kubo formula when an open boundary condition is applied.

*changmingqi@njjust.edu.cn

†shengli@nju.edu.cn

For a Weyl semimetal with two Weyl nodes, the Chern number between the two Weyl nodes is nontrivial. The edge states will form the Fermi arc surface states on the surfaces parallel to the direction of the separation of Weyl nodes. When a magnetic field parallel to the direction of the separation of Weyl nodes is applied, the nonzero Chern number can be obtained from Landau levels. The surface states give rise to a nonzero Hall conductivity for the Fermi energy at the Weyl nodes. For the surfaces perpendicular to the direction of the separation of Weyl nodes, the edge states disappear when the Fermi energy is at the Weyl nodes. The Chern number is zero and the conductivity of the surface is zero when a magnetic field perpendicular to the direction of the separation of the Weyl nodes is applied. Therefore, the Hall conductivity in Weyl semimetals is anisotropic. Our study demonstrates the 3D QHE from the perspective of the bulk-edge correspondence.

The rest of the paper is organized as follows. In Sec. II, we introduce the model Hamiltonian and illustrate the bulk-edge correspondence for 3D QHE in Weyl semimetals. In Sec. III, we plot the energy spectrum of Landau levels and derive the Hall conductivity according to the Chern number from Landau levels. In Sec. IV, we calculate the Hall conductivity in a Weyl semimetal slab with the open boundary condition when a magnetic field is applied. The final section contains a brief summary.

II. ILLUSTRATION OF BULK-EDGE CORRESPONDENCE IN WEYL SEMIMETAL

We consider a 3D model of a Weyl semimetal with two Weyl nodes [11,42–46],

$$H = A(k_x\sigma_x + k_y\sigma_y) + M(k_w^2 - \mathbf{k}^2)\sigma_z, \quad (1)$$

where $(\sigma_x, \sigma_y, \sigma_z)$ are the Pauli matrices, and $\mathbf{k} = (k_x, k_y, k_z)$ is the wave vector. A , M , and k_w are the model parameters. This model contains all the topological properties of Weyl semimetals [46]. The energy dispersion of this model is

$$E_{\pm}^{\mathbf{k}} = \pm\sqrt{A^2(k_x^2 + k_y^2) + M^2(k_w^2 - \mathbf{k}^2)^2}, \quad (2)$$

with \pm for the conductance and valence bands. The model has two Weyl nodes at $\mathbf{k}_{\pm} = (0, 0, \pm k_w)$ with the same energy $E_w = 0$.

The Chern number of this model for a given k_z can be obtained. For $M > 0$, $C_{k_z} = -1$ for $-k_w < k_z < k_w$, and $C_{k_z} = 0$ for other cases. Here, C_{k_z} is the total Chern number of all the occupied electron states below the Fermi energy at a fixed k_z . The nonzero Chern number corresponds to the Fermi arc edge states according to the bulk-boundary correspondence.

In Fig. 1, we plot the energy spectrum of the Weyl semimetal in the momentum space and the Fermi arc surface states in the real space to illustrate the bulk-edge correspondence in Weyl semimetals. The two Weyl nodes are located at the z direction. The Chern number between the two Weyl nodes is nonzero. For the surface parallel to the z direction, the projection of two Weyl nodes on the surface forms Fermi arc states when the Fermi energy is at the Weyl nodes. The Fermi arc states on the opposite surfaces can form a complete Fermi loop supporting the QHE. For the surface perpendicular to the

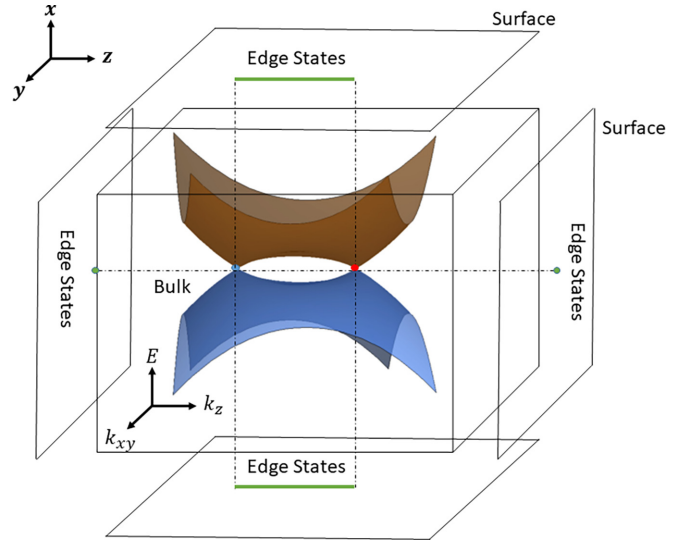


FIG. 1. The energy spectrum of the Weyl semimetal in momentum space, and the illustration of surface states in real space. The Weyl nodes are labeled as red and blue points. The edge states are labeled on the surface as green lines and points.

z direction, the projection of two Weyl nodes is a point when the Fermi energy is at the Weyl nodes. The QHE cannot occur in this situation. Therefore, the QHE in Weyl semimetals is anisotropic.

III. CHERN NUMBERS FROM BULK LANDAU LEVELS

Here we discuss the case in which the magnetic field is perpendicular to the z direction, such as along the y direction. In Fig. 1, the edge state on the x - z plane is a point for Fermi energy at the Weyl nodes. As shown in our previous work [20], the zero Landau levels intersect at the Weyl nodes. The total Chern number is zero for the Fermi energy at the Weyl nodes. According to the bulk-edge correspondence, the Hall conductivity should be zero, which is not our focus.

When a magnetic field along the z direction is applied, the energy spectrum is quantized to Landau bands dispersing with k_z . The vector potential under the Landau gauge is $\mathbf{A} = (0, Bx, 0)$. Using the Peierls transformation, the wave vector is replaced,

$$\mathbf{k} = \left(k_x, k_y + \frac{x}{\ell_B^2}, k_z \right), \quad (3)$$

with $\ell_B^2 = \hbar/|eB|$. We introduce the ladder operators

$$a = \frac{\ell_B}{\sqrt{2}} \left[k_x - i \left(k_y + \frac{x}{\ell_B^2} \right) \right], \quad (4)$$

$$a^\dagger = \frac{\ell_B}{\sqrt{2}} \left[k_x + i \left(k_y + \frac{x}{\ell_B^2} \right) \right]. \quad (5)$$

With the ladder operators, the Hamiltonian Eq. (1) can be written as

$$H = \begin{bmatrix} -\omega_M(a^\dagger a + \frac{1}{2}) - M_k & \frac{\sqrt{2}}{\ell_B} A a \\ \frac{\sqrt{2}}{\ell_B} A a^\dagger & \omega_M(a^\dagger a + \frac{1}{2}) + M_k \end{bmatrix} \quad (6)$$

with $\omega_M = 2M/\ell_B^2$, $M_k = M k_z^2 - M k_w^2$.

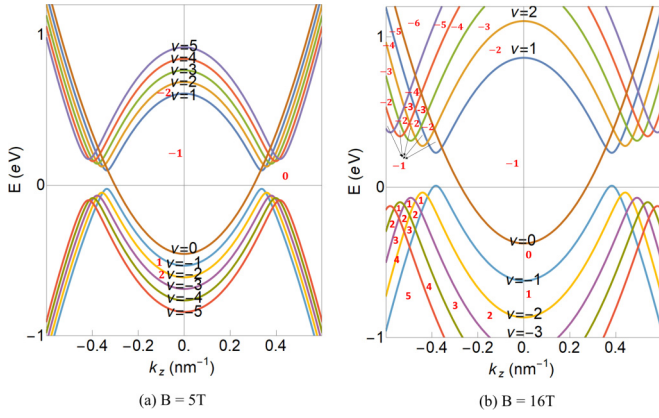


FIG. 2. In a Weyl semimetal slab, the energy spectrum of Landau levels as a function of the wave vector k_z . The Landau levels are labeled in the figure. The Chern numbers C_{k_z} of different regions enclosed by Landau levels are labeled in the figure as red numbers. The parameters are $M = 5 \text{ eV nm}^2$, $A = 0.5 \text{ eV nm}$, and $k_w = \pi/10 \text{ nm}^{-1}$.

The eigenenergies of the Landau levels can be solved as

$$E_{\nu, k_z} = \begin{cases} \frac{\omega_M}{2} + M_k, & \nu = 0, \\ \frac{\omega_M}{2} + \text{sgn}(\nu) \sqrt{\frac{2A}{l_B^2} |\nu| + M_\nu^2}, & \nu \neq 0, \end{cases} \quad (7)$$

with $M_\nu = M_k + \omega_M |\nu|$.

In Fig. 2, we plot the $\nu = 0$ and $\nu = \pm(1, 2, 3, 4, 5)$ Landau levels for magnetic field $B = 5 \text{ T}$ and $B = 16 \text{ T}$. The Chern numbers labeled in the figure can be obtained through topological analyses as shown in our previous work [20].

Let us focus on Fig. 2(a). We consider (E_F, k_z) as a pair of variable parameters, which designates an observation point. We consider a point $(0,0)$ as the observation point. At $B = 0$, the Chern number at $(0,0)$ is -1 according to the result in Sec. II. When the magnetic field B is applied, while the energy spectrum evolves into Landau levels, no Landau level band crosses the observation point $(0,0)$. Therefore, the value of the Chern number at the observation point is unchanged at $B = 5 \text{ T}$. Because the closed region between $\nu = 0$ and $\nu = 1$ Landau levels is connected to the point $(0,0)$, the whole region shares the same Chern number $C_{k_z} = -1$ as labeled in Fig. 2.

Next, we consider an observation point at $E_F = 0$ on the left of the Weyl nodes at $B = 0$. Apparently, the Chern number is $C_{k_z} = 0$ at this point. When magnetic field B is increased continuously to a finite value, the Chern number on this point is unchanged because no Landau level moves across this observation point in this process. As a result, the Chern number in the regions between the $\nu = 0$ and $\nu = -1$ Landau levels connecting to the observation point without crossing the Landau levels is $C_{k_z} = 0$. Then, apparently, if we move an observation point from a $C_{k_z} = 0$ region to a $C_{k_z} = -1$ region, the point must cross upward from below a Landau level. This indicates that the Chern number decreases by 1 when the observation point crosses upward a Landau level from below. Therefore, we can determine the Chern numbers in different regions. We label the Chern numbers in different regions as shown in Fig. 2. In Fig. 2(b), the detailed distribution of Chern numbers has been shown in the left regions.

In Fig. 2(b), the magnetic field is $B = 16 \text{ T}$. Comparing with the case $B = 5 \text{ T}$, the spacing between the Landau levels is wider. The value of the Chern numbers C_{k_z} in different regions is unchanged because the whole region shares the same Chern number. However, the total Chern number at a fixed Fermi energy is changed. Therefore, the Hall conductivity will depend on the magnetic field.

We consider a Weyl semimetal slab with the periodic boundary condition in the z direction. The thickness along the z direction is L_z . Then, the wave vector k_z is discrete, given by $k_z = 2\pi i/L_z$ with i an integer. The Hall conductivity and the Chern number have the relation

$$\sigma_{xy} = n \frac{e^2}{h}, \quad (8)$$

where $n = \sum_{k_z} C_{k_z}$ is the total Chern number of all the occupied electron states below the Fermi energy, and the total Chern number can be calculate by counting the Chern numbers C_{k_z} of all allowed k_z at a special Fermi energy. Here, C_{k_z} is the total Chern number of all the occupied electron states below the Fermi energy at a fixed k_z . For example, for Fermi energy at E_F , the distribution of Chern numbers at E_F can be read in Fig. 2. Therefore, we can get the Chern number carried by each allowed k_z . Then, the total Chern number at E_F can be got by counting all the Chern numbers carried by all allowed k_z at E_F . Therefore, we can calculate the Hall conductivity according to the distribution of Chern numbers in different regions shown in Fig. 2.

First, we calculate the Hall conductivity as a function of magnetic field. Take the Fermi energy at the Weyl nodes, $E_F = 0$, as an example. In Fig. 2(a), $B = 5 \text{ T}$, only the Chern number between the $n = 0$ Landau level is $C_{k_z} = -1$. The Chern number is zero in other areas. At $E_F = 0$, the Chern number carried by each k_z lying between the intersection of the $E_F = 0$ Fermi energy and $\nu = 0$ Landau levels is -1 . To calculate the Chern number, we can only count the allowed k_z between the intersection of the $E_F = 0$ Fermi energy and $\nu = 0$ Landau levels and times -1 ,

$$n_0 = -1 \times \text{Int} \left(\sqrt{k_w^2 - \frac{1}{l_B^2}} \times \frac{L_z}{\pi} \right), \quad (9)$$

with $\text{Int}(\dots)$ taking the integer part of a real number.

As the magnetic field increases continuously, the magnetic field will reach to a series of critical values $B_{c1}, B_{c2}, B_{c3}, \dots$, in which the $\nu = -1, \nu = -2, \nu = -3, \dots$ Landau levels will cross the Fermi energy $E_F = 0$. The critical value B_{c1} can be calculated by solving the equation

$$\text{Max}[E_{-i, k_z}(B_{ci})] = 0, \quad i = 1, 2, 3, \dots \quad (10)$$

For the magnetic field $B_{c1} < B < B_{c2}$ as shown in Fig. 2(b), the $\nu = -2$ Landau level crosses the Fermi energy $E_F = 0$. The region enclosed by the $\nu = -1$ and the $\nu = -2$ Landau levels in which the Chern number is $C_{k_z} = 1$ should be taken into account. To calculate the Chern number n , we should count the k_z with Chern number $C_{k_z} = -1$ and $C_{k_z} = 1$.

To count the k_z with Chern number $C_{k_z} = 1$, we should solve the intersections of the eigenenergies of the $\nu = -1$ Landau level and $E_F = 0$. For a magnetic field $B_{c1} < B < B_{c2}$, we can get four solutions k_{zi} , with $i = 1, 2, 3, 4$, by solving the

equation

$$E_{-1,k_z}(B) = 0. \quad (11)$$

k_{z1} and k_{z4} , k_{z2} and k_{z3} , are symmetric about $k_z = 0$. Hence,

$$n_1 = 1 \times \left[\text{Int} \left(\frac{k_{z2} L_z}{\pi} \right) - \text{Int} \left(\frac{k_{z1} L_z}{\pi} \right) \right]. \quad (12)$$

The total Chern number is

$$n = n_0 + n_1 \quad (13)$$

for the magnetic field $B_{c1} < B < B_{c2}$.

As the magnetic field increases, other regions enclosed by the Landau levels should be considered. The relevant Chern number can be calculated through a similar method. The total Chern number can be obtained as

$$n = n_0 + n_1 + \dots + n_j, \quad B_{cj} < B < B_{C(j+1)} \quad (14)$$

with

$$n_j = C_{k_z} \times \left[\text{Int} \left(\frac{k_{z2}^j L_z}{\pi} \right) - \text{Int} \left(\frac{k_{z1}^j L_z}{\pi} \right) \right]. \quad (15)$$

Here, k_{zi}^j , $i = 1, 2$, $j = 1, 2, 3, \dots$, denote the points of intersection of the energy of $\nu = -j$ Landau levels and Fermi energy.

We have considered the Hall conductivity as a function of magnetic field at $E_F = 0$ above. Now, we consider the Hall conductivity as a function of Fermi energy. Take the magnetic field $B = 16$ T as an example. When the Fermi energy is in the gap between the $\nu = -1$ and $\nu = 1$ Landau levels, only the Chern number C_{k_z} in the region enclosed by the $\nu = 0$ and $\nu = 1$ Landau levels is nonzero. The total Chern number can be calculated by

$$n_0 = -1 \times \text{Int} \left(\sqrt{\frac{E_F}{M} + k_w^2} - \frac{1}{l_B^2} \times \frac{L_z}{\pi} \right), \quad (16)$$

for $E_{-1} < E_F < E_1$, with $E_1 = \text{Min}[E_{1,k_z}]$ and $E_{-1} = \text{Max}[E_{-1,k_z}]$.

For Fermi energy $E_{-2} < E_F < E_{-1}$, with $E_{-2} = \text{Max}[E_{-2,k_z}]$, the region enclosed by the $\nu = -1$ and $\nu = -2$ Landau levels should be considered in which the Chern number for each k_z is $C_{k_z} = 1$. The total Chern number can be calculated by $n = n_0 + n_1$, with

$$n_1 = 1 \times \left[\text{Int} \left(\frac{k_{z2}^{-1} L_z}{\pi} \right) - \text{Int} \left(\frac{k_{z1}^{-1} L_z}{\pi} \right) \right], \quad (17)$$

where k_{zi}^{-1} , with $i = 1, 2, 3, 4$, can be got by solving the equation

$$E_{-1,k_z}(B) - E_F = 0. \quad (18)$$

For $E_1 < E_F < E_{01}$, with E_{01} the energy in which the $\nu = 0$ and $\nu = 1$ Landau levels intersect, the small region enclosed by the $\nu = 0$, $\nu = 1$, and $\nu = 2$ Landau levels should be considered in which the Chern number for each k_z is $C_{k_z} = -1$. The total Chern number can be calculated by $n = n_0 + n_1$, with

$$n_1 = -1 \times \left[\text{Int} \left(\frac{k_{z2}^1 L_z}{\pi} \right) - \text{Int} \left(\frac{k_{z1}^1 L_z}{\pi} \right) \right], \quad (19)$$

where k_{zi}^1 , with $i = 1, 2, 3, 4$, can be got by solving the equation

$$E_{1,k_z}(B) - E_F = 0. \quad (20)$$

For $E_{01} < E_F < E_2$, with $E_2 = \text{Min}[E_{2,k_z}]$, the region enclosed by the $\nu = 0$, $\nu = 1$, and $\nu = 2$ Landau levels should be considered in which the Chern number for each k_z is $C_{k_z} = -1$ in the two small region and $C_{k_z} = -2$ in the one large region. The total Chern number can be calculated by $n = n_0 + n_1 + n_2$, with

$$n_1 = -1 \times \left[\text{Int} \left(\frac{k_{z1}^0 L_z}{\pi} \right) - \text{Int} \left(\frac{k_{z1}^1 L_z}{\pi} \right) \right] \quad (21)$$

and

$$n_2 = -2 \times \left[\text{Int} \left(\frac{k_{z2}^1 L_z}{\pi} \right) - \text{Int} \left(\frac{k_{z1}^0 L_z}{\pi} \right) \right]. \quad (22)$$

Here, k_{zi}^0 , with $i = 1, 2$, can be got by solving the equation

$$E_{0,k_z}(B) - E_F = 0. \quad (23)$$

As the Fermi energy crosses more Landau levels, more regions with different Chern numbers need to be taken into account. The total Chern number can be calculated by counting the allowed C_{k_z} in the different regions.

IV. HALL CONDUCTIVITY

Now, we numerically calculate the Hall conductivity of a Weyl semimetal slab with the open boundary condition in a magnetic field using the Kubo formula

$$\sigma_{\alpha,\beta} = \frac{e^2 \hbar}{iV_{\text{eff}}} \sum_{\delta,\delta' \neq \delta} \frac{\langle \Psi_\delta | v_\alpha | \Psi_{\delta'} \rangle \langle \Psi_{\delta'} | v_\beta | \Psi_\delta \rangle f_{\delta'\delta}}{(E_\delta - E_{\delta'})(E_\delta - E_{\delta'} + i\Gamma)}, \quad (24)$$

where $\alpha, \beta = x, y, z$, $|\Psi_\delta\rangle$ is the eigenstate of energy E_δ for H in a magnetic field, V_{eff} is the volume of the slab, v_α and v_β are the velocity operators, $f_{\delta'\delta} = f(E_{\delta'}) - f(E_\delta)$, and $f(x)$ is the Fermi distribution. The disorder can be introduced in the Kubo formula via the level broadening Γ . For a small Γ , the Hall conductivity can be obtained as the real part of Eq. (24).

The sheet Hall conductivity for the Weyl semimetal slab is defined by $\sigma_H^S = \sigma_H L$. We numerically calculate the sheet Hall conductivity at zero temperature using the same method as [11,47] as shown in the Appendix.

For the magnetic field along the y direction, the Hall conductivity has been calculated in Ref. [11] and our previous work [21]. In our previous work, we got the zero Hall conductivity for the Fermi energy at the Weyl nodes, which is consistent with the bulk-edge correspondence above. When the magnetic field is perpendicular to the Weyl node line, the Hall conductivity of the model Hamiltonian without anisotropic terms is zero for the Fermi energy at the Weyl nodes as shown in our previous work [21]. This is because the total Chern number is zero for the Fermi energy at the Weyl nodes.

For the magnetic field along the z direction, in Fig. 3, we plot the Hall conductivity as a function of Fermi energy at $B = 5$ T. The green line is plotted using the Chern number from the Landau levels. The red line is plotted using the

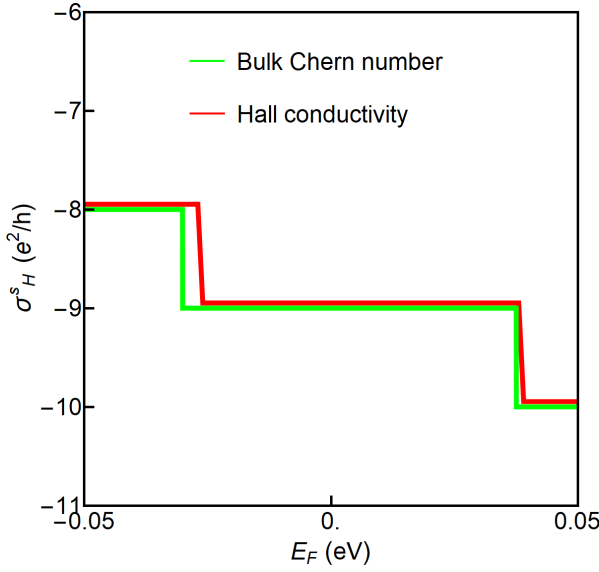


FIG. 3. The sheet Hall conductivity σ_s^H as a function of Fermi energy E_F at $B = 5$ T and $\Gamma = 0$. The red line is calculated using the Kubo formula Eq. (24) and the green line is calculated using the Chern number Eq. (14). The parameters are $M = 5$ eV nm², $A = 0.5$ eV nm, $L_z = 100$ nm, and $k_w = \pi/10$ nm⁻¹.

Kubo formula. In Fig. 3, the numerical results using the Kubo formula are basically consistent with the calculations using the Chern number.

In Fig. 4, we plot the Hall conductivity as a function of magnetic field at $E_F = 0$ eV. The green line and blue line are plotted using the Chern number from the Landau levels,

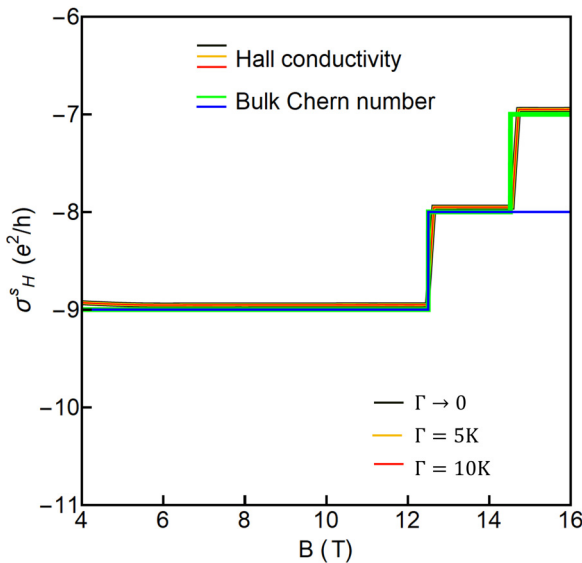


FIG. 4. The sheet Hall conductivity σ_s^H as a function of magnetic field B at $E_F = 0$ eV and $\Gamma = 0$ (black line), 5 K (yellow line), 10 K (red line). The black line, yellow line, and red line are calculated using the Kubo formula Eq. (24), the blue line is calculated using the Chern number Eq. (9), and the green line is calculated using the Chern number Eq. (13). The parameters are $M = 5$ eV nm², $A = 0.5$ eV nm, $L_z = 100$ nm, and $k_w = \pi/10$ nm⁻¹.

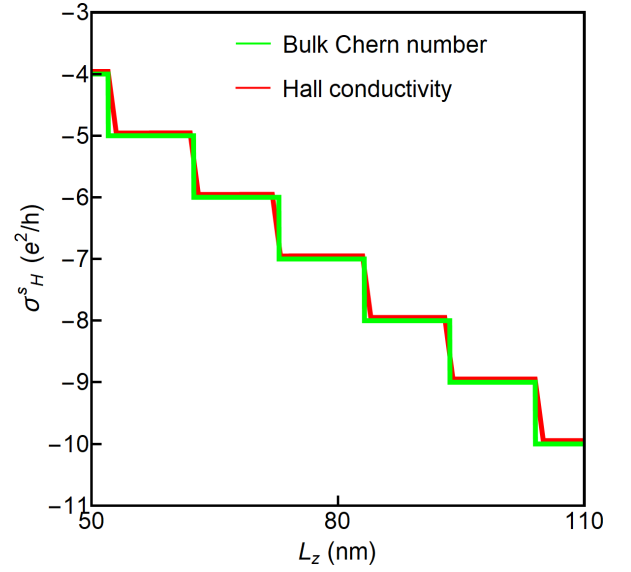


FIG. 5. The sheet Hall conductivity σ_s^H as a function of the thickness of the slab at $B = 5$ T, $E_F = 0$ eV, and $\Gamma = 0$. The red line is calculated using the Kubo formula Eq. (24) with $\Gamma = 0$, and the green line is calculated using the Chern number Eq. (9). The parameters are $M = 5$ eV nm², $A = 0.5$ eV nm, and $k_w = \pi/10$ nm⁻¹.

and the black line, yellow line, and red line are plotted using the Kubo formula with different Γ . The green line is plotted using Eq. (13) and the blue line is plotted using Eq. (9). When the magnetic field $B < B_{c1}$, the blue line is consistent with the Hall conductivity using the Kubo formula. As the magnetic field increase continuously, the two lines begin to deviate when $B > B_{c1}$. Therefore, we can use Eq. (9) only when $B < B_{c1}$. For the case in which the maximum magnetic field in Fig. 4 is $B = 16$ T $< B_{c2}$, we can use Eq. (13) to calculate the Hall conductivity. The results obtained by the Chern numbers are basically consistent with the results using the Kubo formula.

In Fig. 5, we plot the Hall conductivity as a function of the thickness of the slab for $B = 5$ T and $E_F = 0$ eV. The red line is plotted using the Kubo formula with $\Gamma = 0$. The green line is plotted using the bulk Chern number Eq. (9). As shown in the figure, the absolute value of the Hall conductivity increases as the thickness of the slab increases. The red line and the green line are basically consistent.

Comparing the results obtained by the bulk Chern number and the Hall conductivity in Figs. 3–5, the steps of the red curves calculated using the Kubo formula seem less sharp than those using the bulk Chern number and sometimes located at slightly shifted fields. This is because in the numerical calculation the Fermi energy, magnetic field, and thickness of the slab are discrete, while in the analytical calculation using the Chern number these values are continuous. Besides, a finite cutoff energy has been used in the calculation of the Kubo formula, which may introduce a small numerical error into the result. Therefore, the steps of the red curves seem less sharp and sometimes located at slightly shifted fields.

In conclusion, the results calculated by the bulk Chern number are nearly consistent with the numerical Hall response calculations except for a certain parameter region as shown

in Figs. 3–5. The reason is that the finite cutoff energy used in the numerical Hall response calculations will introduce a small numerical error, leading to the discrepancy between the two approaches. Therefore, the analytical bulk Chern number results are more suitable.

V. SUMMARY

In summary, we demonstrate the bulk-edge correspondence for 3D QHE in Weyl semimetals. We first illustrate the relationship between the surface states and bulk topology in Weyl semimetals. When a magnetic field is applied, we calculate the Chern number of a Weyl semimetal slab with the periodic boundary condition through topological analysis. For the surfaces parallel to the direction of the separation of Weyl nodes, the edge states form the Fermi arc surface states due to the topology of the bulk. When a magnetic field parallel to the direction of the separation of Weyl nodes is applied, the nonzero Chern number can be obtained from bulk states. The surface states can give rise to a nonzero Hall conductivity for the Fermi energy at Weyl nodes. For the surfaces perpendicular to the direction of the separation of Weyl nodes, the Chern number is zero, leading to the edge states disappearing. Therefore, for the Fermi energy at Weyl nodes, the Hall conductivity is zero when the magnetic field perpendicular to the direction of the separation of Weyl nodes is applied. We also numerically calculate the Hall conductivity of a Weyl semimetal slab with the open boundary condition. The numerical results are nearly consistent with the analytic Chern numbers. Our study demonstrates the distinct bulk-edge correspondence for the 3D QHE in Weyl semimetals.

ACKNOWLEDGMENT

This work was supported by the National Natural Science Foundation of China under Grants No. 11974168 (L.S.) and No. 12274235 (R.M.).

APPENDIX

To numerically calculate the Hall conductivity for magnetic field along the z direction, we use the bases $|s, \nu, \phi_n\rangle =$

$|\chi_s\rangle \otimes |\nu\rangle \otimes |\phi_n\rangle$, where $|\nu\rangle$ is the harmonic oscillator eigenfunction, and

$$\chi_1 = \begin{bmatrix} 1 \\ 0 \end{bmatrix}, \quad \chi_2 = \begin{bmatrix} 0 \\ 1 \end{bmatrix}, \quad (\text{A1})$$

and

$$\phi_n(z) = \sqrt{\frac{2}{L_z}} \sin \left[\frac{n\pi}{L_z} \left(z + \frac{L}{2} \right) \right], \quad n = 0, 1, 2, \dots \quad (\text{A2})$$

The matrix elements of the Hamiltonian Eq. (6) under the bases are

$$\begin{aligned} & \langle 1, \nu, \varphi_m | H | 1, \nu', \varphi_n \rangle \\ &= \left\{ M \left[k_w^2 - \frac{n^2 \pi^2}{L_z^2} - \frac{2}{\ell_B^2} \left(\nu + \frac{1}{2} \right) \right] \right\} \delta_{\nu\nu'} \delta_{mn}, \end{aligned} \quad (\text{A3})$$

$$\langle 1, \nu, \varphi_m | H | 2, \nu', \varphi_n \rangle = \frac{\sqrt{2}}{l_B} A \sqrt{\nu} \delta_{\nu\nu'+1} \delta_{mn}, \quad (\text{A4})$$

$$\langle 2, \nu, \varphi_m | H | 1, \nu', \varphi_n \rangle = \frac{\sqrt{2}}{l_B} A \sqrt{\nu+1} \delta_{\nu\nu'-1} \delta_{mn}, \quad (\text{A5})$$

$$\begin{aligned} & \langle 2, \nu, \varphi_m | H | 2, \nu', \varphi_n \rangle \\ &= - \left\{ M \left[k_w^2 - \frac{n^2 \pi^2}{L_z^2} - \frac{2}{\ell_B^2} \left(\nu + \frac{1}{2} \right) \right] \right\} \delta_{\nu\nu'} \delta_{mn}. \end{aligned} \quad (\text{A6})$$

We numerically calculate the eigenenergies and eigenstates of the Hamiltonian matrix and the wave function for an eigenstate of energy E_δ as

$$\Psi_\delta(x, z) = \sum_{s, \nu, n} C_{\delta, s\nu n} \varphi_\nu(x) \phi_n(z), \quad (\text{A7})$$

where $\{C_{\delta, s\nu n}\}$ are the superposition coefficients and $\varphi_\nu(x) = \langle x | \nu \rangle$.

With the help of the ladder operators, the velocity is

$$v_x = \frac{A}{\hbar} \sigma_x - \frac{\sqrt{2}M}{\ell_B \hbar} (a^\dagger + a) \sigma_z, \quad (\text{A8})$$

$$v_y = \frac{A}{\hbar} \sigma_y + \frac{\sqrt{2}Mi}{\ell_B \hbar} (a^\dagger - a) \sigma_z. \quad (\text{A9})$$

With the wave function of the Hamiltonian, the matrix elements of the velocity operators are given as

$$\begin{aligned} \langle \Psi_\delta | v_x | \Psi_{\delta'} \rangle &= \frac{1}{\hbar} \sum_{\nu, \nu', n} \left\{ -C_{\delta, 1\nu n}^* C_{\delta', 1\nu' n} \left[\frac{\sqrt{2}M}{\ell_B} (\sqrt{\nu} \delta_{\nu, \nu'+1} + \sqrt{\nu+1} \delta_{\nu, \nu'-1}) \right] \right. \\ &\quad \left. + C_{\delta, 2\nu n}^* C_{\delta', 2\nu' n} \left[\frac{\sqrt{2}M}{\ell_B} (\sqrt{\nu} \delta_{\nu, \nu'+1} + \sqrt{\nu+1} \delta_{\nu, \nu'-1}) \right] + C_{\delta, 1\nu n}^* C_{\delta', 2\nu' n} A \delta_{\nu, \nu'} + C_{\delta, 2\nu n}^* C_{\delta', 1\nu' n} A \delta_{\nu, \nu'} \right\} \delta_{k_y, k'_y}, \end{aligned} \quad (\text{A10})$$

$$\begin{aligned} \langle \Psi_\delta | v_y | \Psi_{\delta'} \rangle &= \frac{1}{\hbar} \sum_{\nu, \nu', n} \left\{ -C_{\delta, 1\nu n}^* C_{\delta', 1\nu' n} \left[\frac{i\sqrt{2}M}{\ell_B} (\sqrt{\nu} \delta_{\nu, \nu'+1} - \sqrt{\nu+1} \delta_{\nu, \nu'-1}) \right] \right. \\ &\quad \left. + C_{\delta, 2\nu n}^* C_{\delta', 2\nu' n} \left[\frac{i\sqrt{2}M}{\ell_B} (\sqrt{\nu} \delta_{\nu, \nu'+1} - \sqrt{\nu+1} \delta_{\nu, \nu'-1}) \right] - iC_{\delta, 1\nu n}^* C_{\delta', 2\nu' n} A \delta_{\nu, \nu'} + iC_{\delta, 2\nu n}^* C_{\delta', 1\nu' n} A \delta_{\nu, \nu'} \right\} \delta_{k_y, k'_y}. \end{aligned} \quad (\text{A11})$$

Substituting the result above into the Kubo formula, we can calculate the Hall conductivity numerically.

- [1] K. v. Klitzing, G. Dorda, and M. Pepper, *Phys. Rev. Lett.* **45**, 494 (1980).
- [2] K. S. Novoselov, A. K. Geim, S. V. Morozov, D. Jiang, M. I. Katsnelson, I. V. Grigorieva, S. V. Dubonos, and A. A. Firsov, *Nature (London)* **438**, 197 (2005).
- [3] Y. Zhang, Y. W. Tan, H. L. Stormer, and P. Kim, *Nature (London)* **438**, 201 (2005).
- [4] R. Yoshimi, K. Yasuda, A. Tsukazaki, K. S. Takahashi, N. Nagaosa, M. Kawasaki, and Y. Tokura, *Nat. Commun.* **6**, 8530 (2015).
- [5] D. J. Thouless, M. Kohmoto, M. P. Nightingale, and M. den Nijs, *Phys. Rev. Lett.* **49**, 405 (1982).
- [6] B. I. Halperin, *Jpn. J. Appl. Phys.* **26**, 1913 (1987).
- [7] M. Kohmoto, B. I. Halperin, and Y.-S. Wu, *Phys. Rev. B* **45**, 13488 (1992).
- [8] M. Koshino, H. Aoki, K. Kuroki, S. Kagoshima, and T. Osada, *Phys. Rev. Lett.* **86**, 1062 (2001).
- [9] B. A. Bernevig, T. L. Hughes, S. Raghu, and D. P. Arovas, *Phys. Rev. Lett.* **99**, 146804 (2007).
- [10] H. L. Störmer, J. P. Eisenstein, A. C. Gossard, W. Wiegmann, and K. Baldwin, *Phys. Rev. Lett.* **56**, 85 (1986).
- [11] C. M. Wang, H.-P. Sun, H.-Z. Lu, and X. C. Xie, *Phys. Rev. Lett.* **119**, 136806 (2017).
- [12] H.-Z. Lu, *Natl. Sci. Rev.* **6**, 208 (2019).
- [13] R. Chen, T. Liu, C. M. Wang, H.-Z. Lu, and X. C. Xie, *Phys. Rev. Lett.* **127**, 066801 (2021).
- [14] P. Wang, Y. Ren, F. Tang, P. Wang, T. Hou, H. Zeng, L. Zhang, and Z. Qiao, *Phys. Rev. B* **101**, 161201(R) (2020).
- [15] F. Qin, S. Li, Z. Z. Du, C. M. Wang, W. Zhang, D. Yu, H.-Z. Lu, and X. C. Xie, *Phys. Rev. Lett.* **125**, 206601 (2020).
- [16] H. Li, H. Liu, H. Jiang, and X. C. Xie, *Phys. Rev. Lett.* **125**, 036602 (2020).
- [17] F. Tang, Y. Ren, P. Wang, R. Zhong, J. Schneeloch, S. A. Yang, K. Yang, P. A. Lee, G. Gu, Z. Qiao *et al.*, *Nature (London)* **569**, 537 (2019).
- [18] R. Chen, C. M. Wang, T. Liu, H.-Z. Lu, and X. C. Xie, *Phys. Rev. Res.* **3**, 033227 (2021).
- [19] R. Ma, D. N. Sheng, and L. Sheng, *Phys. Rev. B* **104**, 075425 (2021).
- [20] M. Chang, H. Geng, L. Sheng, and D. Y. Xing, *Phys. Rev. B* **103**, 245434 (2021).
- [21] M. Chang, Y. Ge, and L. Sheng, *Chin. Phys. B* **31**, 057304 (2022).
- [22] X.-X. Zhang and N. Nagaosa, *Nano Lett.* **22**, 3033 (2022).
- [23] F. Xiong, C. Honerkamp, D. M. Kennes, and T. Nag, *Phys. Rev. B* **106**, 045424 (2022).
- [24] X. Wan, A. M. Turner, A. Vishwanath, and S. Y. Savrasov, *Phys. Rev. B* **83**, 205101 (2011).
- [25] A. A. Burkov and L. Balents, *Phys. Rev. Lett.* **107**, 127205 (2011).
- [26] K. Y. Yang, Y. M. Lu, and Y. Ran, *Phys. Rev. B* **84**, 075129 (2011).
- [27] G. Xu, H. Weng, Z. Wang, X. Dai, and Z. Fang, *Phys. Rev. Lett.* **107**, 186806 (2011).
- [28] P. Delplace, J. Li, and D. Carpentier, *Europhys. Lett.* **97**, 67004 (2012).
- [29] J. H. Jiang, *Phys. Rev. A* **85**, 033640 (2012).
- [30] B. Singh, A. Sharma, H. Lin, M. Z. Hasan, R. Prasad, and A. Bansil, *Phys. Rev. B* **86**, 115208 (2012).
- [31] J. Liu and D. Vanderbilt, *Phys. Rev. B* **90**, 155316 (2014).
- [32] D. Bulmash, C.-X. Liu, and X.-L. Qi, *Phys. Rev. B* **89**, 081106(R) (2014).
- [33] N. P. Armitage, E. J. Mele, and A. Vishwanath, *Rev. Mod. Phys.* **90**, 015001 (2018).
- [34] C. Zhang, A. Narayan, S. Lu, J. Zhang, H. Zhang, Z. Ni, X. Yuan, Y. Liu, J.-H. Park, E. Zhang *et al.*, *Nat. Commun.* **8**, 1272 (2017).
- [35] C. Zhang, Y. Zhang, X. Yuan, S. Lu, J. Zhang, A. Narayan, Y. Liu, H. Zhang, Z. Ni, R. Liu *et al.*, *Nature (London)* **565**, 331 (2019).
- [36] S. Nishihaya, M. Uchida, Y. Nakazawa, M. Kriener, Y. Kozuka, Y. Taguchi, and M. Kawasaki, *Sci. Adv.* **4**, eaar5668 (2018).
- [37] M. Uchida, Y. Nakazawa, S. Nishihaya, K. Akiba, M. Kriener, Y. Kozuka, A. Miyake, Y. Taguchi, M. Tokunaga, N. Nagaosa *et al.*, *Nat. Commun.* **8**, 2274 (2017).
- [38] T. Schumann, L. Galletti, D. A. Kealhofer, H. Kim, M. Goyal, and S. Stemmer, *Phys. Rev. Lett.* **120**, 016801 (2018).
- [39] D. A. Kealhofer, L. Galletti, T. Schumann, A. Suslov, and S. Stemmer, *Phys. Rev. X* **10**, 011050 (2020).
- [40] B.-C. Lin, S. Wang, S. Wiedmann, J.-M. Lu, W.-Z. Zheng, D. Yu, and Z.-M. Liao, *Phys. Rev. Lett.* **122**, 036602 (2019).
- [41] Y. Hatsugai, *Phys. Rev. Lett.* **71**, 3697 (1993).
- [42] S.-B. Zhang, H.-Z. Lu, and S.-Q. Shen, *New J. Phys.* **18**, 053039 (2016).
- [43] S.-Q. Shen, *Topological Insulators* (Springer, Berlin, 2012).
- [44] H.-P. Sun and H.-Z. Lu, *Front. Phys.* **14**, 33405 (2019).
- [45] R. Okugawa and S. Murakami, *Phys. Rev. B* **89**, 235315 (2014).
- [46] H. Z. Lu, S. B. Zhang, and S. Q. Shen, *Phys. Rev. B* **92**, 045203 (2015).
- [47] M. Chang and L. Sheng, *Phys. Rev. B* **103**, 245409 (2021).